Closed-Form Access Probability Analysis for LoRa-Based LEO Satellite IoT

Quantao Yu*, Deepak Mishra†, Hua Wang*, Dongxuan He*, Jinhong Yuan†, and Michail Matthaiou‡
*School of Information and Electronics, Beijing Institute of Technology, Beijing, China
†School of Electrical Engineering and Telecommunications, University of New South Wales, Sydney, Australia
‡Centre for Wireless Innovation (CWI), Queen's University Belfast, BT3 9DT Belfast, U.K.
3120215432@bit.edu.cn, d.mishra@unsw.edu.au, wanghua@bit.edu.cn, dongxuan_he@bit.edu.cn,
j.yuan@unsw.edu.au, m.matthaiou@qub.ac.uk

***Abstract*—Long-range (LoRa) can provide highly energy-efficient and cost-effective communications for low power wide area networks, playing an indispensable role in the Internet of Things (IoT). However, terrestrial LoRa networks cannot guarantee pervasive connectivity, especially in rural and remote areas. To tackle this problem, exploiting LoRa-based low Earth orbit (LEO) satellite IoT has garnered a growing interest in both academia and industry. In this paper, we provide a novel analytical framework based on spherical stochastic geometry (SG) for characterizing the uplink access probability of LoRa-based LEO satellite IoT. For practical modeling, multiple classes of LoRa end-devices (EDs) are taken into consideration, where each class of EDs is modeled by an independent Poisson point process (PPP). Both the channel characteristics of near-Earth satellite communications and the unique features of LoRa network are considered to derive closed-form analytical expressions for the uplink access probability. Numerical simulations validate the accuracy of our theoretical analysis and provide insightful guidelines for the practical design and implementation of LoRa-based LEO satellite IoT.**

***Index Terms*—Access probability, Internet of remote things, LoRa, near-Earth satellite communications, stochastic geometry.**

I. Introduction

A. Background

THE recent years have witnessed the proliferation of LoRa technology in the IoT space, which can be categorized into two layers: a robust physical (PHY) layer using chirp spread spectrum (CSS) modulation and a simple medium access control (MAC) layer with ALOHA-based LoRaWAN protocol [1]. Facilitated by its configurable radio parameters, including carrier frequency, bandwidth, spreading factor, and code rate, LoRa promises a compelling trade-off between data rate and coverage, thus satisfying various requirements of IoT applications [1]. In particular, exploiting LoRa-based LEO satellite IoT has been regarded as a promising solution to the Internet of remote things, and some experiments have already verified the feasibility of LoRa-based radio links in near-Earth satellite communications [2]–[4]. Moreover, some international organizations and satellite companies, like Inmarsat and Lacuna Space, have participated in LoRa-based satellite IoT industrial initiatives over the past few years [5]. However, little attention has been paid to a holistic performance analysis of LoRa-based LEO satellite IoT in terms of access probability, which is of paramount importance for the practical design and implementation of such a specific paradigm.

This work was partially funded by the Australian Research Council (ARC) Discovery Early Career Researcher Award (DECRA) - DE230101391; and was supported in part by the China Scholarship Council (CSC).

The work of M. Matthaiou was supported by the European Research Council (ERC) under the European Union's Horizon 2020 research and innovation programme (grant agreement No. 101001331).

B. State-of-the-Art

Recently, analytical modelling based on SG has been shown to be viable for satellite IoT networks, which paves the way to study the generic performance of satellite IoT networks without relying on specialized software platforms [6]. For example, the authors in [7] developed an analytical model to investigate the uplink performance of satellite IoT networks and derived the analytical expressions for the normalized throughput. Moreover, the authors in [8] put forth an analytical framework and analyzed the coverage performance in terms of frame success rate, which can improve the IoT-over-satellite connectivity by leveraging time diversity, i.e., frame repetition. Besides, the authors in [9] proposed a star-of-star topology to effectively leverage the benefits of multiple satellites, i.e., spatial diversity, to achieve the desired performance in LEO satellite IoT networks. Although these works have laid a solid foundation for the performance evaluation of satellite IoT networks, none of them focuses on the network modelling and performance analysis of LoRa-based LEO satellite IoT. To the best of our knowledge, the most relevant works in the literature are [10] and [11]. However, the system model presented in [10] inherently follows the terrestrial LoRa network paradigm, which limits its findings in the LEO satellite IoT scenarios, while the system model proposed in [11] does not take into account the unique features of LoRa network.

C. Motivation and Contributions

To fill this gap, we present a novel analytical framework for LoRa-based LEO satellite IoT in this paper, which enables a rigorous analysis in terms of uplink access probability that accurately characterizes the link-level performance of such a specific paradigm and thereby facilitates its practical design and implementation. The main contributions of this paper are summarized as follows:

ICC 2025 - IEEE International Conference on Communications | 979-8-3315-0521-9/25/$31.00 ©2025 IEEE | DOI: 10.1109/ICC52391.2025.11161458

1) A new analytical framework for the uplink access probability of LoRa-based LEO satellite IoT is developed based on spherical SG. Both the channel characteristics of near-Earth satellite communications and the unique features of LoRa network are incorporated into our system model.
2) To give a comprehensive performance analysis of LoRa-based LEO satellite IoT, closed-form analytical expressions for the uplink access probability are derived by utilizing the Laplace transform (LT) of the aggregated interference.
3) Numerical simulations are conducted to verify the accuracy of our theoretical analysis, which can provide insightful guidelines for the practical design and implementation of LoRa-based LEO satellite IoT.

II. System Model

A. Network Model

In this paper, we consider a single LEO satellite that directly communicates with the terrestrial LoRa EDs within its coverage region.

1) Geometric model: Without loss of generality, we denote H as the orbit height of the LEO satellite while the terrestrial LoRa EDs are randomly and uniformly distributed within its coverage region, i.e., satellite footprint $\mathcal{R}$, which is determined by the effective beamwidth of serving satellite. Accordingly, we denote the satellite effective beamwidth as ψ, which corresponds to the maximum satellite-centric angle as depicted in Fig. 1. Moreover, to simplify the mathematical representation, we use the contact angle φ to denote the relative location between a LoRa ED and serving satellite, i.e., the Earth-centered zenith angle. According to the basic sine theorem, the maximum contact angle φ_m can be derived as [12]

$$\varphi_m = \begin{cases} \sin^{-1}\left(\frac{R+H}{R}\sin\left(\frac{\psi}{2}\right)\right) - \frac{\psi}{2}, & \text{if } \psi < \psi_0 \\ \cos^{-1}\left(\frac{R}{R+H}\right), & \text{if } \psi \geq \psi_0, \end{cases} \tag{1}$$

where R is the radius of Earth and $\psi_0 = 2\sin^{-1}\left(\frac{R}{R+H}\right)$ denotes the effective beamwidth corresponding to just covering the horizon. As a result, the coverage area of the satellite footprint can be obtained as [13]

$$|\mathcal{R}| = 2\pi R^2 \left(1 - \cos\varphi_m\right). \tag{2}$$

Given the contact angle φ, the distance between the ED and serving satellite, i.e., contact distance, can be obtained using the basic cosine theorem as

$$d\left(\varphi\right) = \sqrt{\left(R+H\right)^2 + R^2 - 2R\left(R+H\right)\cos\varphi}. \tag{3}$$

2) ED model: Let us consider that there are $\mathcal{K}$ classes of LoRa EDs uniformly distributed within the satellite footprint. Each class of EDs is assigned with one spreading factor (SF) and modelled by a PPP Φ_k with intensity λ_k where $k \in \{7, ..., 12\}$ denotes the SF. As a result, the number of EDs of class k is a Poisson random variable, and its mean value can be computed using (2) as

$$\bar{N}_k = \lambda_k |\mathcal{R}| = 2\pi\lambda_k R^2 \left(1 - \cos\varphi_m\right). \tag{4}$$

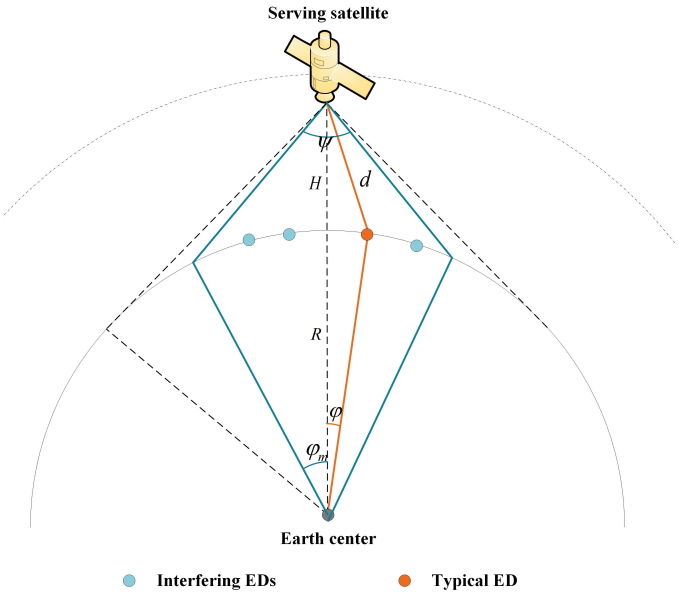

Fig. 1. An illustration of the geometric model of LoRa-based LEO satellite IoT, including the satellite footprint, the effective beamwidth ψ, the contact angle φ, and the contact distance d.

In addition, we assume that different SFs are quasi-orthogonal and thus inter-SF interference can be negligible [14], [15].[1] All classes of EDs are equipped with an omni-directional antenna with the same effective isotropic radiated power (EIRP) denoted as P_t. Moreover, we denote Φ_k^A as the set of active EDs of class k, which also follows a PPP with intensity $p_k\lambda_k$, where $p_k = \frac{T_k}{T_p}$ is the active probability of class k with T_k and T_p representing the Time on Air (ToA) of class k and the average packet inter-arrival time, respectively.

Specifically, the configurations of bandwidth, SF, and code rate impact the ToA of class k, which can be formulated as [15]

$$T_k = \left(N_{pre} + 4.25 + N_{pay}\right)\frac{2^k}{B_W}, \tag{5}$$

where B_W is the configured bandwidth, N_{pre} and N_{pay} denote the number of CSS symbols in the preamble and the PHY payload, respectively, with N_{pay} being calculated as [15]

$$N_{pay} = \max\left\{\left\lceil\frac{8P_L - 4k + 28 + 16C - 20H_E}{4k}\right\rceil\left(C_R + 4\right), 0\right\} + 8, \tag{6}$$

where P_L denotes the PHY payload length in bytes, $C_R \in \{1, 2, 3, 4\}$ denotes the code rate, C indicates the presence (i.e., $C = 1$) or absence (i.e., $C = 0$) of cyclic redundancy check (CRC), while $H_E = 0$ indicates that the PHY layer

[1]It has been shown in [14] that interfering EDs with different SFs have an average rejection signal-to-interference ratio threshold of -16 dB. Therefore, different SFs can be considered to be quasi-orthogonal in LoRa systems [15]. Hence, we only consider the impact of dominant same SF (co-SF) interference in this paper.

header is enabled whereas $H_E = 1$ indicates that the PHY layer header is not enabled.

B. Channel Model

In this paper, both large-scale fading and small-scale fading are taken into consideration.

1) Large-scale fading: For the sake of simplicity, we adopt the free space path-loss model to characterize the large-scale fading, which is suitable for the Internet of remote things where the EDs are typically distributed in open remote areas (e.g., forests, deserts, and oceans) [16]. Specifically, given the transmission distance $d(\varphi)$ and the carrier frequency f_c, the free space path-loss is given by

$$L(d(\varphi)) = \left(\frac{c}{4\pi f_c d(\varphi)}\right)^2, \tag{7}$$

where c refers to the speed of light.

2) Small-scale fading: Let us denote $h_{o,k}$ and $h_{i,k}$ as the small-scale fading from the typical and interfering devices of class k to the serving satellite, respectively, which follows an independent and identically distributed (i.i.d.) shadowed Rician (SR) fading with Nakagami fading coefficient m, the half average power of scattered component b_0 and the average power of line-of-sight component Ω. As such, the cumulative distribution function (CDF) and probability density function (PDF) for all the SR channel gains $|h|^2$ are given by [17]

$$F_{|h|^2}(x) = \left(\frac{2b_0 m}{2b_0 m + \Omega}\right)^m \sum_{z=0}^{\infty} \frac{(m)_z}{z!\Gamma(z+1)} \left(\frac{\Omega}{2b_0 m + \Omega}\right)^z \times \gamma\left(z+1, \frac{1}{2b_0}x\right), \tag{8}$$

$$f_{|h|^2}(x) = \left(\frac{2b_0 m}{2b_0 m + \Omega}\right)^m \frac{1}{2b_0} \exp\left(-\frac{x}{2b_0}\right) \times {}_1F_1\left(m, 1, \frac{\Omega x}{2b_0(2b_0 m + \Omega)}\right), \tag{9}$$

respectively, where $\Gamma(\cdot)$ denotes the Gamma function, $\gamma(\cdot,\cdot)$ is the lower incomplete Gamma function, $(\cdot)_z$ is the Pochhammer symbol, while ${}_1F_1(\cdot,\cdot,\cdot)$ is the confluent hypergeometric function. Note that (8) and (9) are too complex to calculate, and thus we approximate the SR channel gain $|h|^2$ by a Gamma random variable with its CDF and PDF denoted as [17]

$$F_{|h|^2}(x) \approx \frac{1}{\Gamma(\alpha)}\gamma\left(\alpha, \frac{x}{\beta}\right), \ x \geq 0, \tag{10}$$

$$f_{|h|^2}(x) \approx \frac{1}{\beta^\alpha \Gamma(\alpha)} x^{\alpha-1} \exp\left(-\frac{x}{\beta}\right), \ x \geq 0, \tag{11}$$

where $\alpha \triangleq \frac{m(2b_0+\Omega)^2}{4mb_0^2+4mb_0\Omega+\Omega^2}$ and $\beta \triangleq \frac{4mb_0^2+4mb_0\Omega+\Omega^2}{m(2b_0+\Omega)}$ denote the shape and scale parameters, respectively.

C. Signal Model

Let us denote $s_{o,k}$ and $s_{i,k}$ as the unit power transmitted signal from the typical and interfering EDs of class k, respectively. Likewise, $\varphi_{o,k}$ and $\varphi_{i,k}$ are the contact angles of the typical and interfering EDs of class k, respectively. Similar to the methods adopted in [7], [12], we denote $\kappa \in [0,1]$ as the interference mitigation factor, which captures the impact of random access on the received signal and underpins the flexibility of performance analysis. In particular, $\kappa = 0$ represents an ideal interference-free system, while $\kappa = 1$ represents the worst-case scenario corresponding to an ALOHA-based system. Consequently, the received signal of class k can be expressed as

$$r_k = \underbrace{\sqrt{P_t G L(d(\varphi_{o,k}))} h_{o,k} s_{o,k}}_{\text{desired signal}} + \underbrace{\kappa \sum_{i \in \Phi_k^A \setminus o} \sqrt{P_t G L(d(\varphi_{i,k}))} h_{i,k} s_{i,k}}_{\text{interfering signal}} + w, \tag{12}$$

where P_t is the EIRP of EDs, G represents the satellite antenna gain and w represents the complex circularly symmetric additive white Gaussian noise (AWGN) with zero mean and variance $\sigma^2 = -174 + N_F + 10\log_{10} B_W$, with N_F representing the receiver's noise figure.

III. Uplink Access Probability Analysis

To evaluate the uplink performance, we define the access probability P_s as the performance metric, which measures the probability of successful transmission, i.e., the desired transmitted signal can be successfully demodulated. For a typical LoRa network, the successful transmission occurs only if both the signal-to-noise ratio (SNR) and the signal-to-interference ratio (SIR) of the received signal exceed their corresponding thresholds. Therefore, the access probability P_s can be defined as [15]

$$P_s = P_{SNR} P_{SIR}, \tag{13}$$

where

$$P_{SNR} = \Pr\left\{\frac{P_t G L(d(\varphi_{o,k}))|h_{o,k}|^2}{\sigma^2} \geq \gamma_k\right\}, \tag{14}$$

and

$$P_{SIR} = \Pr\left\{\frac{L(d(\varphi_{o,k}))|h_{o,k}|^2}{\kappa \sum_{i \in \Phi_k^A} L(d(\varphi_{i,k}))|h_{i,k}|^2} \geq \gamma_I\right\}, \tag{15}$$

denote the *connection probability* and the *capture probability*, respectively, γ_k is the SF-specific SNR threshold, while γ_I is the capture effect (CE) threshold.

A. Connection Probability

Particularly, the connection probability can be derived as

$$\begin{aligned} P_{SNR} &= \Pr\left\{|h_{o,k}|^2 \geq \frac{\sigma^2 \gamma_k}{P_t G L(d(\varphi_{o,k}))}\right\} \\ &= 1 - F_{|h_{o,k}|^2}\left(\frac{\sigma^2 \gamma_k}{P_t G L(d(\varphi_{o,k}))}\right) \\ &\overset{(a)}{\approx} 1 - \frac{1}{\Gamma(\alpha)}\gamma\left(\alpha, \frac{\sigma^2 \gamma_k}{\beta P_t G L(d(\varphi_{o,k}))}\right), \end{aligned} \tag{16}$$

where step (a) follows directly from the substitution of the CDF described in (10). Note that P_{SNR} is related to the link budget and is independent of the ED's intensity.

B. Capture Probability

To facilitate analysis, the capture probability defined in (15) can be rewritten as

$$\begin{aligned} P_{SIR} =& \Pr\left\{\frac{P_t G L\left(d\left(\varphi_{o,k}\right)\right)\left|h_{o,k}\right|^2}{I_k} \geq \gamma_I\right\} \\ =& 1-\underbrace{\Pr\left\{\left|h_{o,k}\right|^2<\frac{I_k \gamma_I}{P_t G L\left(d\left(\varphi_{o,k}\right)\right)}\right\}}_{P_o}. \end{aligned} \tag{17}$$

Note that P_o cannot be directly computed due to the randomness of both channel fading and aggregated interference. To address this issue, we first introduce Alzer's lemma in the following proposition.

Proposition 1. *Let g be a Gamma random variable with the shape parameter α and the scale parameter β. Its CDF can be tightly bounded as*

$$\begin{cases} F_g(x) \leq [1-\exp(-\mu x)]^\alpha, & \text{if } \alpha \leq 1 \\ F_g(x) > [1-\exp(-\mu x)]^\alpha, & \text{if } \alpha > 1, \end{cases} \tag{18}$$

where $\mu = (\alpha!)^{-\frac{1}{\alpha}}/\beta$ and the equality holds when $\alpha = 1$.

For more details regarding the accuracy of this approximation, please refer to [17], [18].

As such, P_o in (17) can be computed as

$$\begin{aligned} P_o =& \Pr\left\{\left|h_{o,k}\right|^2<\frac{I_k \gamma_I}{P_t G L\left(d\left(\varphi_{o,k}\right)\right)}\right\} \\ \overset{(b)}{\approx}& \mathbb{E}_{I_k}\left[\left[1-\exp\left(-\frac{\mu I_k \gamma_I}{P_t G L\left(d\left(\varphi_{o,k}\right)\right)}\right)\right]^\alpha\right] \\ \overset{(c)}{=}& \mathbb{E}_{I_k}\left[\sum_{z=0}^{\infty}\binom{\alpha}{z}(-1)^z \exp\left(-\frac{z\mu I_k \gamma_I}{P_t G L\left(d\left(\varphi_{o,k}\right)\right)}\right)\right] \\ \overset{(d)}{=}& \sum_{z=0}^{\infty}\binom{\alpha}{z}(-1)^z \mathcal{L}_{I_k}(s), \end{aligned} \tag{19}$$

where $s = \frac{z\mu\gamma_I}{P_t G L(d(\varphi_{o,k}))}$, $\mathbb{E}[\cdot]$ denotes the expectation operation, step (b) follows the approximated CDF of Gamma random variable according to Alzer's lemma introduced in Proposition 1, step (c) follows the generalized binomial theorem and step (d) follows the LT for I_k. Note that the LT of a random variable X is defined as $\mathcal{L}_X(\nu) = \mathbb{E}\left[e^{-\nu X}\right]$ with $\nu \in \mathbb{C}$.

Herein, we provide a brief explanation of the reason for the convergence of the infinite series in (19). According to Jensen's inequality [19], we have

$$\begin{aligned} &\mathbb{E}_{I_k}\left[-\exp\left(-\frac{\mu I_k \gamma_I}{P_t G L\left(d\left(\varphi_{o,k}\right)\right)}\right)\right] \\ &\leq \underbrace{-\exp\left(-\frac{\mu \bar{I}_k \gamma_I}{P_t G L\left(d\left(\varphi_{o,k}\right)\right)}\right)}_{\mathcal{I}_I}, \end{aligned} \tag{20}$$

with

$$\begin{aligned} \left|\mathcal{I}_I\right| \overset{(e)}{\approx}& \exp\left(-\frac{\mu\pi R\kappa p_k \lambda_k \alpha\beta \ln\left(\frac{v_2}{v_1}\right)\gamma_I\left[d\left(\varphi_{o,k}\right)\right]^2}{R+H}\right) \\ \overset{(f)}{\leq}& \exp\left(-\frac{\mu\pi R\kappa p_k \lambda_k \alpha\beta \ln\left(\frac{v_2}{v_1}\right)\gamma_I H^2}{R+H}\right) < 1, \end{aligned} \tag{21}$$

where $v_1 = H^2$, $v_2 = (R+H)^2 + R^2 - 2R(R+H)\cos\varphi_m$, step (e) follows from the derivation of $\bar{I}_k = \mathbb{E}[I_k]$ as shown in the Appendix, while step (b) follows from the fact that the contact angle $\varphi_{o,k} \in [0, \varphi_m]$ as stated in Section II. This guarantees the convergence of the infinite series in (19) according to the convergence property of binomial series [19] and thus validates the effectiveness of our derived analytical expressions of the capture probability. The convergence of this infinite series will also be demonstrated by numerical simulations in Section IV.

Subsequently, to derive the analytical expression of P_{SIR}, we first need to calculate the LT of I_k, which is presented as follows

$$\begin{aligned} \mathcal{L}_{I_k}(s) =& \mathbb{E}_{I_k}\left[\exp\left(-s\sum_{i\in\Phi_k^A\setminus o}\kappa P_t G L\left(d\left(\varphi_{i,k}\right)\right)\left|h_{i,k}\right|^2\right)\right] \\ =& \mathbb{E}_{I_k}\left[\prod_{i\in\Phi_k^A\setminus o}\exp\left(-s\kappa P_t G L\left(d\left(\varphi_{i,k}\right)\right)\left|h_{i,k}\right|^2\right)\right] \\ \overset{(g)}{=}& \mathbb{E}_{\Phi_k^A\setminus o}\left[\prod_{i\in\Phi_k^A\setminus o}\left[1+s\beta\kappa P_t G L\left(d\left(\varphi_{i,k}\right)\right)\right]^{-\alpha}\right], \end{aligned} \tag{22}$$

where step (g) follows from the independence of the i.i.d. channel fading and random point process and leverages the moment generating function (MGF) of a Gamma random variable.

According to the probability generating functional (PGFL) of PPP [20], we have

$$\mathbb{E}\left[\prod_{x\in\Phi} f(x)\right] = \exp\left(-\int_{\mathbb{R}^d}\left[1-f(x)\right]\Lambda(\mathrm{d}x)\right), \tag{23}$$

where Φ is a point process on $\mathbb{R}^d$ and $\Lambda(\cdot)$ is the intensity measure of Φ.

As a result, $\mathcal{L}_{I_k}(s)$ can be further formulated as

$$\begin{aligned} \mathcal{L}_{I_k}(s) =& \mathbb{E}\left[\prod_{i\in\Phi_k^A\setminus o}\left[1+s\beta\kappa P_t G L\left(d\left(\varphi_{i,k}\right)\right)\right]^{-\alpha}\right] \\ \overset{(h)}{=}& \exp\Big\{2\pi R^2 p_k\lambda_k \times \\ & \underbrace{\int_0^{\varphi_m}\left(\left[1+s\beta\kappa P_t G L\left(d\left(\varphi\right)\right)\right]^{-\alpha}-1\right)\sin\varphi \mathrm{d}\varphi}_{\mathcal{I}_{II}}\Big\}, \end{aligned} \tag{24}$$

where step (h) leverages the PGFL of the PPP as described

in (23), whilst the integral part $\mathcal{I}_{II}$ can be derived as

$$\begin{aligned}\mathcal{I}_{II} &= \int_0^{\varphi_m} \left(\left[1 + s\beta\kappa P_t G L\left(d\left(\varphi\right)\right)\right]^{-\alpha} - 1 \right) \sin\varphi \mathrm{d}\varphi \\ &= \int_0^{\varphi_m} \frac{\sin\varphi}{\left(1 + \frac{\epsilon}{\delta + \cos\varphi}\right)^{\alpha}} \mathrm{d}\varphi + \cos\varphi_m - 1 \\ &\overset{(i)}{=} \int_{\delta+\cos\varphi_m}^{\delta+1} \frac{1}{\left(1 + \frac{\epsilon}{u}\right)^{\alpha}} \mathrm{d}u + \cos\varphi_m - 1 \\ &= t_1 \left[\frac{\left(\frac{t_1}{\epsilon}\right)^{\alpha} {}_2F_1\left(\alpha, \alpha+1; \alpha+2; -\frac{t_1}{\epsilon}\right)}{\alpha+1} - 1 \right] - \\ &\quad t_2 \left[\frac{\left(\frac{t_2}{\epsilon}\right)^{\alpha} {}_2F_1\left(\alpha, \alpha+1; \alpha+2; -\frac{t_2}{\epsilon}\right)}{\alpha+1} - 1 \right], \end{aligned} \quad (25)$$

where $\epsilon = -\frac{s\beta\kappa P_t G c_0^2}{2R(R+H)}$ with $c_0 = \frac{c}{4\pi f_c}$, $\delta = -\frac{(R+H)^2+R^2}{2R(R+H)}$, step (i) follows from $u = \delta + \cos\varphi$, $t_1 = 1 - \frac{(R+H)^2+R^2}{2R(R+H)}$, $t_2 = \cos\varphi_m - \frac{(R+H)^2+R^2}{2R(R+H)}$, while ${}_2F_1\left(\cdot,\cdot;\cdot;\cdot\right)$ is the Gaussian hypergeometric function [19].

Therefore, the capture probability can be formulated according to (17), (19), and (24) as

$$\begin{aligned} P_{SIR} &= 1 - P_o \\ &\approx 1 - \sum_{z=0}^{\infty} \binom{\alpha}{z} (-1)^z \mathcal{L}_{I_k}(s) \\ &= 1 - \sum_{z=0}^{\infty} \binom{\alpha}{z} (-1)^z \exp\left(2\pi R^2 p_k \lambda_k \mathcal{I}_{II}\right). \end{aligned} \quad (26)$$

C. Access Probability

Accordingly, the closed-form analytical expression of the uplink access probability P_s is given in the following proposition.

Proposition 2. *The closed-form analytical expression of the uplink access probability P_s is approximately given by*

$$\begin{aligned} P_s \approx & \left[1 - \frac{1}{\Gamma(\alpha)} \gamma\left(\alpha, \frac{\sigma^2 \gamma_k}{\beta P_t G L\left(d\left(\varphi_{o,k}\right)\right)}\right)\right] \\ & \times \left[1 - \sum_{z=0}^{\infty} \binom{\alpha}{z} (-1)^z \exp\left(2\pi R^2 p_k \lambda_k \times \right.\right. \\ & \left.\left. \left(t_1 \left[\frac{\left(\frac{t_1}{\epsilon}\right)^{\alpha} {}_2F_1\left(\alpha, \alpha+1; \alpha+2; -\frac{t_1}{\epsilon}\right)}{\alpha+1} - 1 \right] - \right.\right.\right. \\ & \left.\left.\left. t_2 \left[\frac{\left(\frac{t_2}{\epsilon}\right)^{\alpha} {}_2F_1\left(\alpha, \alpha+1; \alpha+2; -\frac{t_2}{\epsilon}\right)}{\alpha+1} - 1 \right] \right) \right) \right]. \end{aligned} \quad (27)$$

Proof: By substituting (16) and (26) into (13), (27) can be obtained. The proof is completed. ∎

IV. Numerical Results and Discussion

In this section, we validate our theoretical performance analysis through Monte-Carlo simulations, which also provide valuable insights into the uplink performance of LoRa-based LEO satellite IoT under practical system parameters. The simulation setup is illustrated as follows. Unless otherwise specified, we set $R = 6371$ km, $P_L = 50$ bytes, $T_p = 3600$ s, $f_c = 868$ MHz, $B_W = 125$ kHz, $P_t = 16$ dBm, $N_F = 6$ dB, $G = 22.6$ dBi, $\psi = 50°$, $\lambda = 10^{-6}$, and $\kappa = 10^{-3}$. Without loss of generality, the contact angle of the desired ED is set to be $0°$. Moreover, we assume that $N_{pre} = 8$, $C = 1$, $H_E = 0$, and $C_R = 1$ as in [15]. The SR fading parameters are set as $m = 5.21$, $b_0 = 0.251$, and $\Omega = 0.278$, which is in accordance with [21]. In addition, the SF-specific SNR threshold γ_k is $-6, -9, -12, -15, -17.5, -20$ dB for k from 7 to 12, respectively, and the CE threshold γ_I is set to be 6 dB [15].

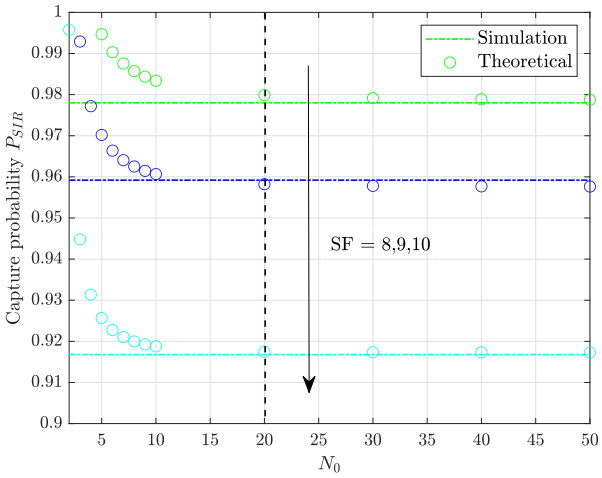

Fig. 2. Theoretical capture probability versus the first N_0 terms used in the calculation of the infinite series.

First, Fig. 2 shows the theoretical capture probability, P_{SIR}, given by (26), versus the first N_0 terms used in the calculation of the infinite series. It can be observed that the theoretical P_{SIR} not only rapidly converges to fixed values due to the relatively small values of system parameters, i.e., α, κ, λ_k, used in our simulations, but also agrees well with the simulation results, which corroborates our analysis.

Figs. 3(a) and 3(b) demonstrate the access probability of different classes of LoRa EDs versus the ED's density for $H = 500$ km and $H = 1000$ km, where the notations "Theoretical" and "Simulation" denote the analytical and numerical results, respectively. Likewise, Figs. 4(a) and 4(b) demonstrate the access probability of different classes of LoRa EDs versus the satellite effective beamwidth for $H = 500$ km and $H = 1000$ km, respectively. The numerical results of access probability are very close to the analytical results given by (27), which substantiates our proposed analytical framework. Furthermore, as illustrated in Fig. 3 and Fig. 4, the access probability is a monotonically decreasing function of both λ and ψ as the interference levels increase with the increase of either λ or ψ. Specifically, the access probability degrades exponentially with the increase of λ, showing that varying the ED's density has a significant impact on the uplink performance of LoRa-based LEO satellite IoT. Notably, the LoRa EDs with larger SF have more severe performance degradation especially for large

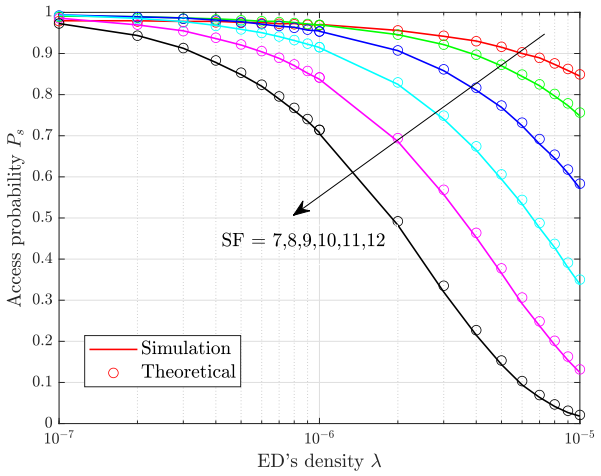

(a) Orbit height $H = 500$ km

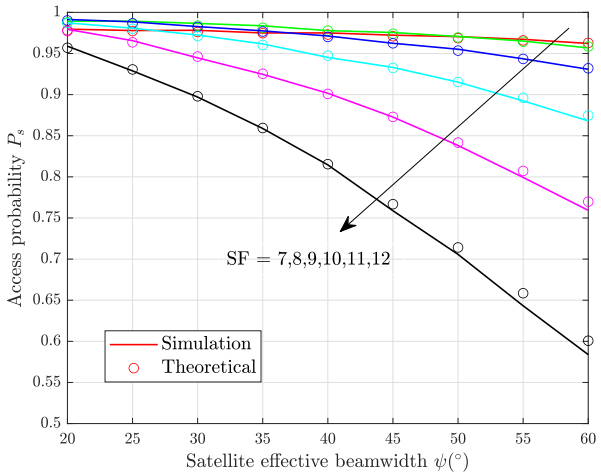

(a) Orbit height $H = 500$ km

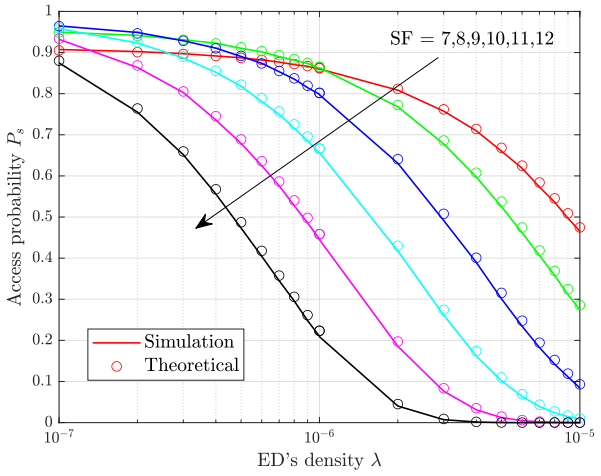

(b) Orbit height $H = 1000$ km

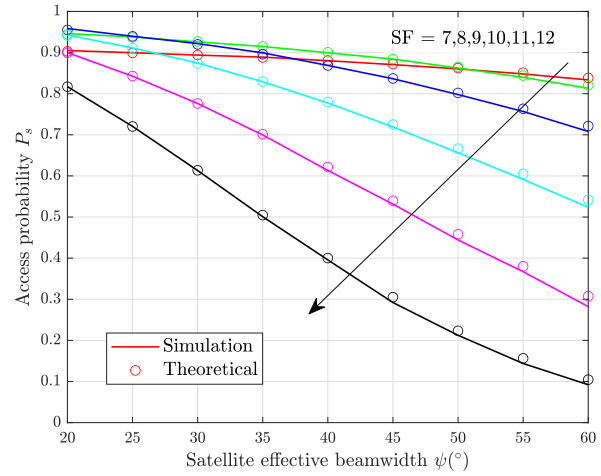

(b) Orbit height $H = 1000$ km

Fig. 3. Access probability of different classes of LoRa EDs versus the ED's density with (a) $H = 500$ km and (b) $H = 1000$ km.

Fig. 4. Access probability of different classes of LoRa EDs versus the satellite effective beamwidth with (a) $H = 500$ km and (b) $H = 1000$ km.

values of ED's density since higher SFs could be more prone to packet collisions due to longer ToA. However, it should be noted that for small values of ED's density, like $\lambda = 10^{-7}$, the access performance of LoRa EDs with smaller SFs could be better than that of LoRa EDs with larger SFs since in this case P_{SNR} will play a dominant role in determining the access probability. Hence, the uplink performance of LoRa-based LEO satellite IoT can be effectively enhanced by tuning both the SF and ED's density according to practical Quality-of-Service (QoS) requirements.

Additionally, it can be observed that the access performance degrades more rapidly for $H = 1000$ km compared to $H = 500$ km due to the escalated large-scale fading. Moreover, as shown in Fig. 4, the orbit height has a more evident impact on the access performance, especially for large satellite effective beamwidth, since for higher orbit, the satellite footprint area increases more rapidly with the increase of ψ, thus leading to more severe aggregated interference and, thus, performance deterioration. This, in turn, indicates that we can control the interference level and optimize the access performance by adjusting the satellite orbit height and effective beamwidth. Therefore, the practical access performance can be improved by reasonable network deployments, including both space and terrestrial segments. As pointed out in [21], [22], the overall network performance can be further enhanced through the dense deployment of LEO satellite constellations, which is an interesting topic for future research. In addition, it is worth noting that addressing some practical challenges, such as Doppler effects associated with synchronization issues, random access combined with interference mitigation techniques, is of great significance to enhance the real-world applicability of LoRa-based LEO satellite IoT systems, which requires

further investigations in the future.

V. Conclusion

In this paper, a novel analytical framework for LoRa-based LEO satellite IoT was formulated based on SG. In particular, both the channel characteristics of near-Earth satellite communications and the unique features of LoRa network were incorporated into the proposed system model, which provided an accurate performance evaluation of such a specific paradigm. Closed-form analytical expressions for the link-level performance were derived in terms of uplink access probability. Numerical simulations were conducted to verify the accuracy of our proposed analytical framework for performance analysis and also provided insightful guidelines for the practical design and implementation of LoRa-based LEO satellite IoT.

Appendix

Recalling the expression of I_k, we have

$$\begin{aligned}\bar{I}_k &= \mathbb{E}_{I_k}\left[\kappa \sum_{i\in\Phi_k^A\setminus o} P_t G L\left(d\left(\varphi_{i,k}\right)\right)\left|h_{i,k}\right|^2\right] \\ &\overset{(j)}{=} 2\pi R^2 \kappa p_k \lambda_k P_t G \int_0^{\varphi_m} L\left(d\left(\varphi\right)\right)\mathbb{E}_{|h|^2}\left[|h|^2\right]\sin\varphi \mathrm{d}\varphi \\ &\overset{(k)}{\approx} 2\pi R^2 \kappa p_k \lambda_k P_t G \alpha\beta \underbrace{\int_0^{\varphi_m} L\left(d\left(\varphi\right)\right)\sin\varphi \mathrm{d}\varphi}_{\mathcal{I}}, \end{aligned} \tag{28}$$

where step (j) follows from the fact that the i.i.d. channel fading is independent of the spatial random point process, while step (k) follows the mean value of the approximated Gamma distribution of channel fading. Moreover, the integral part $\mathcal{I}$ can be derived as

$$\begin{aligned}\mathcal{I} &= \int_0^{\varphi_m} L\left(d\left(\varphi\right)\right)\sin\varphi \mathrm{d}\varphi \\ &\overset{(l)}{=} \int_{\cos\varphi_m}^{1} \frac{\left(\frac{c}{4\pi f_c}\right)^2}{\left(R+H\right)^2 + R^2 - 2R\left(R+H\right)u}\mathrm{d}u \\ &\overset{(m)}{=} \int_{v_1}^{v_2} \frac{c_0^2}{2R\left(R+H\right)v}\mathrm{d}v \\ &= \frac{c_0^2}{2R\left(R+H\right)}\ln\left(\frac{v_2}{v_1}\right), \end{aligned} \tag{29}$$

where step (l) follows from the substitution $u = \cos\varphi$, while step (m) follows by using $v = \left(R+H\right)^2 + R^2 - 2R\left(R+H\right)u$.

Consequently, by substituting (29) into (28), $\bar{I}_k$ can be obtained as

$$\bar{I}_k \approx \pi R \kappa p_k \lambda_k P_t G \alpha\beta \left(\frac{c_0^2 \ln\left(\frac{v_2}{v_1}\right)}{R+H}\right). \tag{30}$$

References

[1] C. Milarokostas, D. Tsolkas, N. Passas, and L. Merakos, "A comprehensive study on LPWANs with a focus on the potential of LoRa/LoRaWAN systems," *IEEE Commun. Surveys Tuts.*, vol. 25, no. 1, pp. 825-867, 1st Quart., 2023.

[2] M. Asad Ullah, G. Pasolini, K. Mikhaylov, and H. Alves, "Understanding the limits of LoRa direct-to-satellite: the Doppler perspectives," *IEEE Open J. Commun. Soc.*, vol. 5, pp. 51-63, Nov. 2023.

[3] F. A. Tondo, M. Afhamisis, S. Montejo-Sánchez, O. L. A. López, M. R. Palattella, and R. D. Souza, "Multiple channel LoRa-to-LEO scheduling for direct-to-satellite IoT," *IEEE Access*, vol. 12, pp. 30627-30637, Feb. 2024.

[4] Y. Xiao, D. Mishra, J. Yuan, and Y. Luo, "Proportionally fair robust beamforming for multicast multibeam satellite systems," *IEEE Commun. Lett.*, vol. 26, no. 1, pp. 128-132, Jan. 2022.

[5] M. Centenaro, C. E. Costa, F. Granelli, C. Sacchi and L. Vangelista, "A survey on technologies, standards and open challenges in satellite IoT," *IEEE Commun. Surveys Tuts.*, vol. 23, no. 3, pp. 1693-1720, 3rd Quart., 2021.

[6] R. Wang, M. A. Kishk, and M. -S. Alouini, "Ultra-dense LEO satellite-based communication systems: A novel modeling technique," *IEEE Commun. Mag.*, vol. 60, no. 4, pp. 25-31, Apr. 2022.

[7] C. C. Chan, B. Al Homssi, and A. Al-Hourani, "A stochastic geometry approach for analyzing uplink performance for IoT-over-satellite," in *Proc. IEEE ICC*, May 2022, pp. 1-6.

[8] B. Manzoor, A. Al-Hourani, and B. A. Homssi, "Improving IoT-over-satellite connectivity using frame repetition technique," *IEEE Wireless Commun. Lett.*, vol. 11, no. 4, pp. 736-740, Apr. 2022.

[9] A. K. Dwivedi, S. Chaudhari, N. Varshney, and P. K. Varshney, "Performance analysis of LEO satellite-based IoT networks in the presence of interference," *IEEE Internet Things J.*, vol. 11, no. 5, pp. 8783-8799, Mar. 2024.

[10] W. Zhou, T. Hong, X. Ding, and G. Zhang, "LoRa performance analysis for LEO satellite IoT networks," in *Proc. IEEE WCSP*, Oct. 2021, pp. 1-5.

[11] A. Talgat, M. A. Kishk, and M. -S. Alouini, "Stochastic geometry-based uplink performance analysis of IoT over LEO satellite communication," *IEEE Trans. Aerosp. Electron. Syst.*, vol. 60, no. 4, pp. 4198-4213, Aug. 2024.

[12] B. A. Homssi and A. Al-Hourani, "Modeling uplink coverage performance in hybrid satellite-terrestrial networks," *IEEE Commun. Lett.*, vol. 25, no. 10, pp. 3239-3243, Oct. 2021.

[13] B. Al Homssi and A. Al-Hourani, "Optimal beamwidth and altitude for maximal uplink coverage in satellite networks," *IEEE Wireless Commun. Lett.*, vol. 11, no. 4, pp. 771-775, Apr. 2022.

[14] D. Croce, M. Gucciardo, S. Mangione, G. Santaromita, and I. Tinnirello, "Impact of LoRa imperfect orthogonality: Analysis of link-level performance," *IEEE Commun. Lett.*, vol. 22, no. 4, pp. 796-799, Apr. 2018.

[15] L. -T. Tu, A. Bradai, Y. Pousset, and A. I. Aravanis, "On the spectral efficiency of LoRa networks: performance analysis, trends and optimal points of operation," *IEEE Trans. Commun.*, vol. 70, no. 4, pp. 2788-2804, Apr. 2022.

[16] M. De Sanctis, E. Cianca, G. Araniti, I. Bisio, and R. Prasad, "Satellite communications supporting Internet of remote things," *IEEE Internet Things J.*, vol. 3, no. 1, pp. 113-123, Feb. 2016.

[17] H. Jia, Z. Ni, C. Jiang, L. Kuang, and J. Lu, "Uplink interference and performance analysis for megasatellite constellation," *IEEE Internet Things J.*, vol. 9, no. 6, pp. 4318-4329, Mar. 2022.

[18] H. Alzer, "On some inequalities for the incomplete Gamma function," *Math. Comput.*, vol. 66, no. 218, pp. 771-778, 1997.

[19] A. Jeffrey and D. Zwillinger, *Table of Integrals, Series, and Products.* Amsterdam, The Netherlands: Elsevier, 2007.

[20] M. Haenggi, *Stochastic Geometry for Wireless Networks*. Cambridge, U.K.: Cambridge Univ. Press, 2012.

[21] H. Jia, C. Jiang, L. Kuang, and J. Lu, "An analytic approach for modeling uplink performance of mega constellations," *IEEE Trans. Vehicular Tech.*, vol. 72, no. 2, pp. 2258-2268, Feb. 2023.

[22] B. Al Homssi *et al.*, "Next generation mega satellite networks for access equality: opportunities, challenges, and performance," *IEEE Commun. Mag.*, vol. 60, no. 4, pp. 18-24, Apr. 2022.